J. theor. Biol. (2000) **206,** 279–290
doi:10.1006/jtbi.2000.2120, available online at http://www.idealibrary.com on IDEAL®

Within-host Spatial Dynamics of Viruses and Defective Interfering Particles

STEVEN A. FRANK*

Department of Ecology and Evolutionary Biology, University of California, Irvine, CA 92697-2525, *U.S.A.*

(*Received on* 2 *August* 1999, *Accepted in revised form on* 2 *June* 2000)

Defective-interfering (DI) viruses arise spontaneously by deletion mutations. The shortened genomes of the DI particles cannot replicate unless they coinfect a cell with a wild-type virus. Upon coinfection, the DI genome replicates more quickly and outcompetes the wild type. The coinfected cell produces mostly DI viruses. At the population level, the abundances of DI and wild-type viruses fluctuate dramatically under some conditions. In other cases, the DI viruses appear to mediate persistent infections with relatively low levels of host cell death. This moderation of viral damage has led some to suggest DI particles as therapeutic agents. Previous mathematical models have shown that either fluctuation or persistence can occur for plausible parameter values. I develop new mathematical models for the population dynamics of DI and wild-type viruses. My work extends the theory by developing specific predictions that can be tested in the laboratory. These predictions, if borne out by experiment, will explain the key processes that control the diversity of observed outcomes. The most interesting prediction concerns the rate at which killed host cells are replaced. A low rate of replacement causes powerful epidemics followed by a crash in viral abundance. As the rate of replacement increases, the frequency of oscillations increases in DI and wild-type viral abundances, but the severity (amplitude) of the fluctuations declines. At higher replacement rates for host cells, nearly all cells become infected by DI particles and a low level of fluctuating, wild-type viremia persists.

Introduction

Viral genomes occasionally produce mutant copies with large deletions. The partially deleted genomes may, for example, lack the coding regions for replication enzymes and capsid proteins. Defective particles of this sort cannot replicate or transmit by themselves. But when they coinfect a cell with normal viruses, defective particles can replicate and coat themselves with products encoded by their partners' genomes (von Magnus, 1954; Huang & Baltimore, 1977; Holland, 1990).

* E-mail: safrank@uci.edu

Defective genomes may gain a replication advantage over the wild type simply because the mutants are shorter. In addition, selection favors defective genomes that outcompete the wild type for replication enzymes and capsid proteins. This competition causes coinfected cells to produce few wild-type viruses and many fully coated, infectious viruses with shortened genomes. The shortened, parasitic genomes are often called defective interfering (DI) particles (Huang & Baltimore, 1977; Barrett & Dimmock, 1986; Roux *et al.*, 1991).

DI particles arise almost invariably during *in vitro* serial passage of RNA viruses with high

0022–5193/00/180279 + 12 $35.00/0

multiplicity of infection per host cell (von Magnus, 1954; Holland, 1990). RNA genomes have high mutation rates, producing many deletion mutants. Frequent coinfection guarantees that shortened, rapidly replicating mutants can parasitize the information of the wild type during coinfection. DNA viruses also produce DI particles under similar conditions, but have not been studied as intensively as RNA genomes (Perrault, 1981).

DI particles have attracted attention for three aspects of population dynamics. First, *in vitro* serial passage often produces dramatic, unpredictable fluctuations in the relative abundances of DI and wild-type viruses (Roux *et al*., 1991; Bangham & Kirkwood, 1993). Second, DI particles can potentially act as therapeutic agents by limiting viral damage to host tissue *in vivo* (Huang & Baltimore, 1977; Cave *et al*., 1984). DI infection by itself appears to be relatively benign. Once host cells are widely infected by DI particles, wild-type virus typically causes superinfection of DI-infected cells. Superinfection produces mostly infectious DI particles. These DI particles infect more cells, making it increasingly difficult for the virulent, wild-type virus to increase in abundance. Third, some authors have suggested that DI particles play an important role in maintaining persistent infections (Holland *et al*., 1980; Barrett & Dimmock, 1986; Chen *et al*., 1996).

Several models have analysed the population dynamics of DI particles. Bangham & Kirkwood (1990), Kirkwood & Bangham (1994) and Szathmáry (1993) showed that fluctuating abundances of DI and wild-type viruses often arise as a result of the "predator–prey" feedback dynamics between wild-type and DI viruses. Prior hypotheses had emphasized special attributes of replication or molecular interaction. The mathematical models were important because they showed that the dynamics arise from universal properties of birth, death, and transmission rather than the special details of the system.

Chen *et al*. (1992) proposed that DI viruses engineered specifically to interfere with HIV-1 replication could be used as therapeutic agents. Nelson & Perelson (1995) developed a numerically realistic model of DI dynamics based on known parameters of HIV infection. They concluded that DI particles are unlikely to survive or to influence HIV dynamics in peripheral blood, but may survive within infected lymphoid organs such as the lymph nodes and spleen.

I develop a model for the population dynamics of wild-type and DI viruses. I extend past models in the following ways. First, I develop a simplified model with only wild-type viruses and host cells. I show that the factors that control oscillations of viral abundance in this simplified model explain most, but not all, of the dynamical properties of the full model with both wild-type and DI viruses. This connection between the simplified model and the full model makes it much easier to understand the processes that control the dynamics in the full model.

Second, I extend the model to analyse the spatial dynamics of viremia. Prior models assumed homogeneous, well-mixed populations of cells, wild-type viruses, and DI particles. My spatial models allow one to compare dynamics under different assumptions about the movement and mixing of viruses and the regeneration of host cells. The methods for spatial modeling provide tools to enhance the study of within-host dynamics for a wide variety of virus–host interactions.

Third, I explore the parameter space to develop comparative predictions about the dynamics of viremia. The prior, generic models of Szathmáry (1993) and Kirkwood & Bangham (1994) showed that oscillations plausibly arise from the intrinsic feedbacks of virus–DI–host interactions, but did not clarify which parameters tend to control the main features of the dynamics. By contrast, the model of Nelson & Perelson (1995) did examine the role of various parameters, but their analysis was specifically designed to study HIV infection of $CD4^+$ cells.

DI particles provide special insight into the within-host dynamics of viral infections. The polymorphism is relatively easy to detect when compared with other types of viral diversity. The DI particles and wild-type viruses differ sharply in their vital demographic characteristics of birth and death rates, and they form a special trophic relationship similar to a predator–prey interaction. RNA viruses generate DI particles *de novo* at a fairly high rate. Thus, even the failure to find a significant number of DI particles provides

bounds on the demographic properties of viruses and host cells.

In short, this striking polymorphism provides a special window onto the dynamics within the host. Such dynamics are undoubtedly very complex. But the models that follow show how increasingly complex systems may sometimes best be studied by first stripping the system to its barest essentials, there to find the simple processes that drive many features of the more complex interactions.

Model

I study the dynamics of free virus and several classes of infected cells. A free virus is either a full particle capable of the complete life cycle by itself, denoted by V, or a DI particle, denoted by D. Cells occur in five varieties: uninfected, C_U; infected only by DI viruses, C_D; infected only by full viruses and early enough in the replication cycle to be interfered by superinfection by a DI virus, C_V; infected only by full viruses and late enough in the replication cycle not to be interfered by superinfection by a DI virus, C_{V^*}; and infected by both full and DI viruses such that the DI viruses can interfere with replication of the full genomes, C_{VD} [see Table 1].

The abundance of the viral and cellular types may vary over space. The abundances in each location depend on both the local interactions of cells and viruses and the movement (diffusion) of viruses from other locations. I assume that cells do not move. The local abundance of each variable is therefore a function of time, t, and spatial location, $\mathbf{x}$, where $\mathbf{x}$ is a location vector in n dimensions. This system forms a classical reaction–diffusion model common in ecological applications (e.g. Segel & Levin, 1976; Hastings, 1978; Allen, 1983; Takeuchi, 1986; Murray, 1989).

TABLE 1
Variables of the model

Variable	Description
V	Abundance of free virus
D	Abundance of defective interfering (DI) virus
C_U	Abundance of uninfected cells
C_D	Abundance of cells infected only by DI viruses
C_V	Abundance of cells infected only by V viruses, early in replication cycle and can be superinfected and interfered by DI viruses
C_{V^*}	Abundance of cells infected only by V viruses, late in replication cycle and cannot be interfered by DI superinfection
C_{VD}	Abundance of cells infected by both V and D viruses, D viruses interfere with replication of V viruses
N	Total abundance of all cell types

The following equations describe this reaction–diffusion system:

$$\frac{\partial V}{\partial t} = \beta\pi_2 C_{V^*} - cV + \delta\nabla^2 V, \tag{1a}$$

$$\frac{\partial D}{\partial t} = \gamma\phi C_{VD} - cD + \delta\nabla^2 D, \tag{1b}$$

$$\frac{\partial C_U}{\partial t} = rC_U(1 - N/K) - k(V + D)C_U + \alpha C_D, \tag{1c}$$

$$\frac{\partial C_D}{\partial t} = kDC_U - \alpha C_D - kVC_D, \tag{1d}$$

$$\frac{\partial C_V}{\partial t} = kVC_U - \pi_1 C_V - kDC_V - \mu C_V, \tag{1e}$$

$$\frac{\partial C_{V^*}}{\partial t} = \pi_1 C_V - \pi_2 C_{V^*}, \tag{1f}$$

$$\frac{\partial C_{VD}}{\partial t} = kVC_D + kDC_V - \phi C_{VD} + \mu C_V, \tag{1g}$$

$$N = C_U + C_D + C_V + C_{V^*} + C_{VD}, \tag{1h}$$

where N is the total number of cells at a location, and ∇^2 terms are the vectors of second partial derivatives in abundance in the n spatial dimensions $(\partial^2/\partial x_1^2, \ldots, \partial^2/\partial x_n^2)$. Roughly speaking, the diffusion terms cause a location's abundance of viruses to be averaged over the abundances of viruses in the neighboring locations. This averaging occurs at a rate set by the diffusion coefficient, δ.

Table 1 summarizes the variables of the model. Table 2 defines the parameters with dimension for each given in terms of time, t, length, L, and number, $\#$.

TABLE 2
Dimensional parameters in order of appearance in eqns (1)

Parameter	Units and description
t	(t), natural time scale
x_i	(L), natural length scale for spatial dimension i
β	($\#/\#$) non-dimensional, number of V viruses produced divided by number of C_{V^*} cells at burst phase
π_2	($1/t$), rate at which C_{V^*} cells burst to produce free virus
c	($1/t$), clearance of free virus (adsorption, decay, antibody clearance, etc.)
δ	(L^2/t), viral diffusion coefficient
γ	($\#/\#$) non-dimensional, number of D viruses produced divided by number of C_{VD} cells at burst phase
ϕ	($1/t$), rate at which C_{VD} cells burst to produce free virus
r	($1/t$), intrinsic rate of increase for C_U cells
K	($\#$), number of cells per location at cellular carrying capacity, determines density-dependent control of cellular proliferation
k	($1/t\#$), rate of infection per virus
α	($1/t$), conversion of C_D cell to C_U cell by loss of DI virus viability in cell without V viruses
π_1	($1/t$), rate at which C_V cells convert to C_{V^*} cells
μ	($1/t$), mutation of V to D viruses within cells, changing a C_V cell into a C_{VD} cell

My model shares several features with the model of Kirkwood & Bangham (1994). Differences include: a spatial component in my model against a single, well-mixed interaction in their model; explicit age structure of infected cells in their model against only two age categories for V infected cells in my model; density-dependent regulation of cellular proliferation in my model vs. uncontrolled growth in the absence of virus in their model; and loss of DI viruses from C_D cells at rate α in my model vs. no loss in theirs.

The system is easier to analyse when rewritten in non-dimensional form (Segel, 1972; Murray, 1989). Non-dimensional analysis focuses attention on a minimal set of parameters and highlights relative magnitudes (scaling relations) among the processes that drive the dynamics. This is accomplished without altering the dynamics or interpretation because one can translate freely between the biologically motivated formulation and the non-dimensional quantities.

Table 3 shows the non-dimensional scalings. I use only the non-dimensional quantities in the

TABLE 3
*Non-dimensional variables and parameters**

Non-dimensional parameter	Scaling of dimensional parameters
$\hat{V}, \hat{D}, \hat{C}_y$	$= Z/K$, where Z is a placeholder for the various viral and cellular abundances, y is a placeholder for various cellular types, and all abundances are expressed in relation to cellular carrying capacity, K, e.g. $\hat{C}_U = C_U/K$
$\hat{t}$	$= ct$, non-dimensional time units expressed as the expected time to clear a free viral particle
$\hat{x}_i$	$= x_i(c/\delta)^{1/2}$, non-dimensional length units expressed as the expected diffusion distance per non-dimensional time unit
$\hat{\pi}_1, \hat{\pi}_2, \hat{\phi}, \hat{\alpha}, \hat{\mu}, \hat{r}$	$= z/c$, where z is a placeholder for various rate parameters scaled to non-dimensional time units, e.g. $\hat{\phi} = \phi/c$
$\hat{k}$	$= kK/c$, infection rate per viral particle adjusted to the non-dimensional scales for time ($1/c$) and abundance (K)
β, γ	Defined originally as non-dimensional parameters

* *Notes*: (a) I use non-dimensional parameters beginning with eqns (2) and following through the remainder of the paper. The hats on the non-dimensional parameters are dropped in the text. (b) The dimensional parameters c, δ, and K are absorbed by the non-dimensional scalings and do not appear in the non-dimensional system in eqns (2).

remainder of the paper unless otherwise noted. With these substitutions, the system in eqns (1) can be rewritten in non-dimensional terms as

$$\frac{\partial V}{\partial t} = \beta\pi_2 C_{V^*} - V + \nabla^2 V, \tag{2a}$$

$$\frac{\partial D}{\partial t} = \gamma\phi C_{VD} - D + \nabla^2 D, \tag{2b}$$

$$\frac{\partial C_U}{\partial t} = rC_U(1 - N) - k(V + D)C_U + \alpha C_D, \tag{2c}$$

$$\frac{\partial C_D}{\partial t} = kDC_U - \alpha C_D - kVC_D, \tag{2d}$$

$$\frac{\partial C_V}{\partial t} = kVC_U - \pi_1 C_V - kDC_V - \mu C_V, \tag{2e}$$

$$\frac{\partial C_{V^*}}{\partial t} = \pi_1 C_V - \pi_2 C_{V^*}, \tag{2f}$$

$$\frac{\partial C_{VD}}{\partial t} = kVC_D + kDC_V - \phi C_{VD} + \mu C_V, \tag{2g}$$

$$N = C_U + C_D + C_V + C_{V^*} + C_{VD}, \tag{2h}$$

where in these equations and in the following I drop the hats from the non-dimensional parameters defined in Table 3. I describe in the Appendix my methods for numerical analysis of these partial differential equations.

Viral Dynamics without DI Particles

I begin analysis with a reduced version of eqns (2). We can prevent the increase of DI particles and the associated variables D, C_D, and C_{VD} by setting to zero the number of DI particles that emerge from jointly infected cells, that is, by setting $\gamma = 0$. The DI particles arise only by mutation in this model, so we may also set $\mu = 0$ to avoid introduction of DI viruses.

These simplifications reduce the system to the four variables V, C_U, C_V, and C_{V^*}. Recall that C_V is a cell newly infected with standard virus and susceptible to disruption by superinfecting DI particles, whereas C_{V^*} cells have maturing viral infections that are no longer susceptible to superinfection. This distinction does not play a role in the absence of DI particles. If we let $\pi_1 \to \infty$, then C_V cells are transformed immediately into C_{V^*} cells. Thus, we may take the burst rate for infected cells as $\pi \approx \pi_2$, dropping C_V from the system. This leaves us with

$$\frac{\partial V}{\partial t} = \beta\pi C_{V^*} - V + \nabla^2 V, \tag{3a}$$

$$\frac{\partial C_U}{\partial t} = rC_U\,(1 - C_U - C_{V^*}) - kVC_U, \tag{3b}$$

$$\frac{\partial C_{V^*}}{\partial t} = kVC_U - \pi C_{V^*}. \tag{3c}$$

If we ignore diffusion, there is a single internal equilibrium at

$$V = \beta\pi C_{V^*}, \tag{4a}$$

$$C_U = 1/k\beta, \tag{4b}$$

$$C_{V^*} = rC_U(1 - C_U)/(rC_U + \pi) \tag{4c}$$

under the assumptions that $\pi \neq 0$ and $k\beta > 1$. I discuss conditions for local stability of this internal equilibrium in the Appendix. Note that we can rescale this system by making the substitution $V = \beta W$, with W as a scaled measure of the abundance of free viruses. This substitution causes the parameters k and β always to appear together as a single parameter, $k\beta$. Thus, apart from scaling, the global dynamics depend only on the three parameters $k\beta$, r, and π.

I studied global dynamics without diffusion numerically in light of the analytical results, and reached three conclusions. (1) The virus is lost when $k\beta < 1$, otherwise as $k\beta$ increases, abundances fluctuate with decreased frequency and increased amplitude of oscillations. (2) Increases in r lead to increased frequency and decreased amplitude of oscillations, with a faster approach to the internal equilibrium when the system is stable. (3) Increases in π from low values cause increased frequency and strongly increased amplitude of oscillations. Further increases create strong transient bursts of virus followed by crashes, leading to local extinction or very long

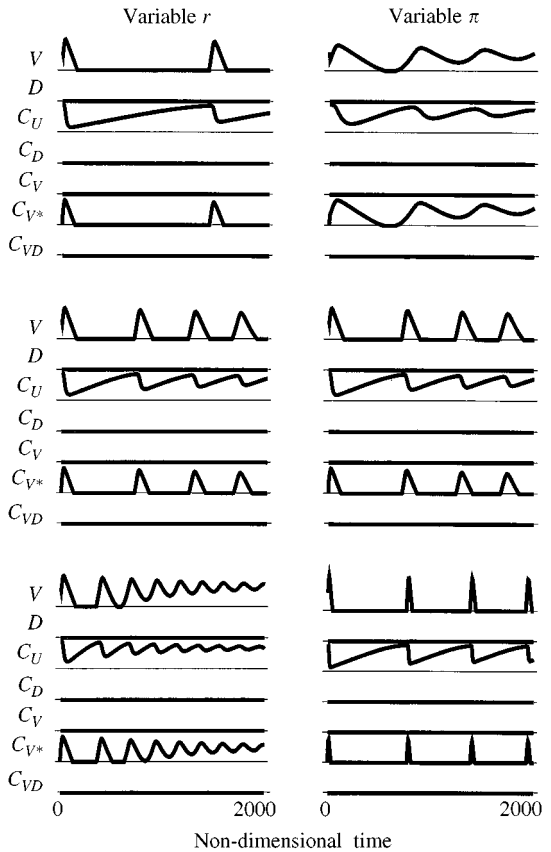

FIG. 1. Time-series plots of the system in eqns (3) without spatial diffusion. Each panel shows the varying abundances of all seven variables from eqns (2), although in this case only V, C_U, C_{V*} vary. I show all variables here for comparison with later figures that plot changes in all seven types. Abundances are plotted on a logarithmic scale, for viruses from 0.01 to 10, and for cells from 0.001 to 1. All variables and parameters are on the non-dimensional scale. The panels compare results for changes in one parameter against a standard set of: $k = 0.01$; $\beta = 600$; $r = 0.01$; and $\pi = 0.07$. The parameter r was varied by a factor of two in the left column, starting at the top with 0.005, in the middle row with 0.01, and at the bottom row with 0.02. The parameter π was varied by a factor of four in the right column, starting at the top with 0.0175, in the middle row with 0.07, and at the bottom row with 0.28. I used a stepsize for each iterate of $\Delta t = 0.1$ over 20,000 iterates, for a total of 2000 non-dimensional time units. I initialized the system with $V = C_U = 1$ and $C_{V*} = 0$. The appendix describes the numerical methods.

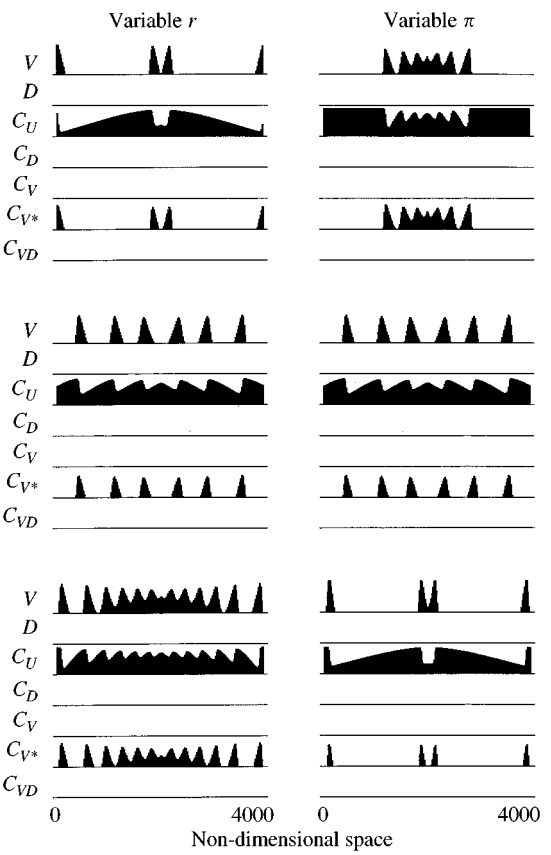

FIG. 2. Spatial pattern of the system in eqns (3) at a single point in time. Arrangement and parameters are the same as in Fig. 1. In addition, the spatial grid has 200 locations, and the distance between locations is $\Delta x = 20$, giving a total non-dimensional length of 4000. The appendix describes the numerical methods.

periods between powerful transient bursts. Figure 1 shows example dynamics for variations in r and π.

I studied the role of spatial interaction with the same system, adding back the diffusion term for V in eqn (3a). Figure 2 shows spatial dynamics for an array of parameters that matches Fig. 1. The time series in Fig. 1 explains most aspects of the spatial dynamics in Fig. 2. For example, increasing r leads to increased frequency and reduced amplitude of oscillations in the time series. These changes correspond to increased frequency and reduced amplitude over time in the spatial waves in the left column of Fig. 2.

Figure 2 shows spatial pattern frozen at a particular point in time. Space occurs in one dimension over a line. To understand these spatial patterns, one must imagine the space–time dynamics as follows. At the start of a run, uninfected cells occur at full abundance over all locations, which would appear as a solid bar over the line for C_U. Also at the start, the abundance of free, wild-type virus, V, is equal to the number of uninfected cells only at the center grid point and

is equal to zero elsewhere. This would appear as a narrow peak for V in the center of the line. The dynamics begin with free virus infecting cells at this center location. The number of infected cells, C_{V^*}, rises and the number of uninfected cells, C_U, declines at the center grid location.

The virus diffuses to neighboring locations, beginning spatial waves that spread from the center in both directions. The waves of viral peaks cause a decline in C_U and a peak in C_{V^*}. At each location, as C_U dips, that location cannot maintain virus, so the peaks in V and C_{V^*} drop and cannot rise again at that location until the uninfected cells (C_U) have recovered. The parameter r determines the rate of recovery of uninfected cells. The net effect is that the peaks in V and C_{V^*} spread from the center, with corresponding valleys in C_U spreading in tandem. At a particular location, the time between peaks declines with an increase in r.

With this method of visualization in mind, one can match the spatial patterns in the left column of Fig. 2 with the temporal patterns in Fig. 1. With low r (top, left panel), recovery takes a long time, causing a low frequency of temporal and spatial waves, each of large amplitude. With increasing r (bottom, left panel), the damped temporal oscillations in Fig. 1 correspond to reduced amplitude spatial waves over time (near the center) in Fig. 2, eventually approaching a nonfluctuating equilibrium over the spatial domain.

Variations in π interact with spatial diffusion in a different way. Lower π corresponds to a longer time between infection and burst production of new virus. Slow production greatly reduces the speed of the spatial waves, thus the low temporal frequency in the upper right panel of Fig. 1 corresponds to closely bunched, slowly moving spatial peaks in the matching panel of Fig. 2. Increasing π causes more rapidly moving spatial waves but also greater local depression of C_U with a passing wave. Thus, a site requires a longer time to recovery before it can support the next wave. High π can lead to global extinction of the virus because rapidly moving waves of infection travel off the end of the line before the center can recover sufficiently to support the next round of infection.

Faster diffusion rates typically cause spatial waves to travel faster. More importantly, high diffusion rates can lead to viral extinction. The key parameter is the length of the spatial domain relative to the diffusion rate. When this length scaling becomes too small, the spatial waves may travel off the ends so quickly that the uninfected cells in the center do not have enough time to recover and generate a new wave before viral extinction. Thus, small organs may be more prone to viral extinctions than large organs.

Dynamics with DI Particles

I return to the full system with DI particles in eqns (2). I present results in this section supporting two conclusions. (1) The frequency of oscillations are driven primarily by the V–C_U–C_{V^*} subsystem summarized in the prior section. (2) The rate of replacement of killed cells, r, dominates the qualitative structure of the full system as in the reduced V–C_U–C_{V^*} subsystem. In the full system, higher values of r lead to dominance of DI particles and a significant reduction in the severity of cellular death caused by viral (V) outbreaks.

Figure 3 shows time series for various parameter combinations without spatial diffusion. The middle panel in the left column matches closely the parameters used for the same panel in the simplified system of Fig. 1. The dynamics are nearly identical—note that the time-scale differs between the figures. Starting with this middle panel in the left column of Fig. 3, we can trace the effects of varying r and α. A decline in r (top-left panel) reduces the frequency of oscillations. A rise in r (lower-left panel) increases the frequency of oscillations and, as in the simpler system, has a tendency toward a damped approach to a steady state.

In the full model shown in Fig. 3, abundances of all classes do not stabilize as quickly with a rise in r as in the simpler system in Fig. 1. Instead, the first effect of rising r in Fig. 3 is an increase in the stable abundance of cells infected by DI (the C_D class). These DI-infected cells prevent the spread of full viruses, V, because when a full virus infects a cell with a latent DI particle, the cell bursts producing only DI progeny. Note that the abundances are on a logarithmic scale; there is only a low frequency of C_{V^*} cells bursting to produce V. Thus, the DI particles protect the

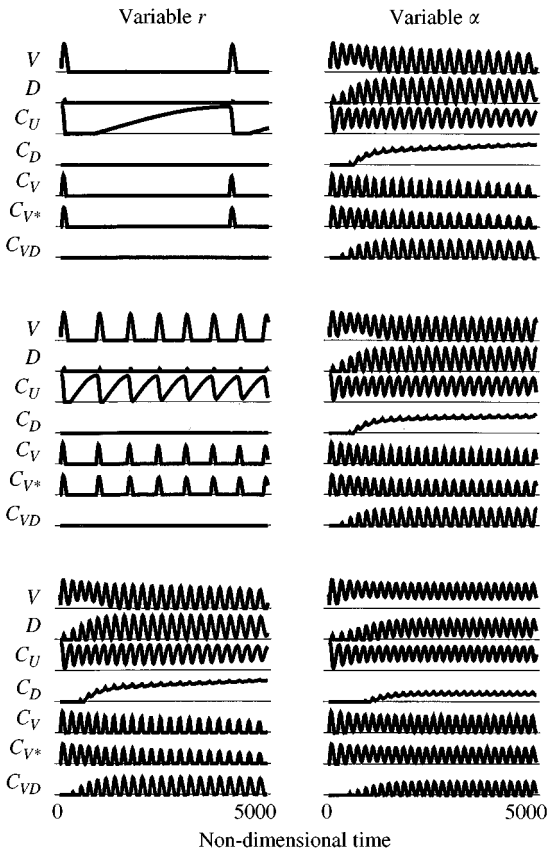

FIG. 3. Time series plots of the system in eqns (2) without spatial diffusion. The structure of the figure and the parameters match Fig. 1, with the following differences. The total time here is 5000 non-dimensional units rather than the 2000 in Fig. 1. Abundance scales here are also logarithmic, but the lower values are 0.1 for viruses and 0.01 for cells; these increases in the lower limits make it easier to see how DI particles reduce viremias to low levels. The base parameters here are: $\pi_1 = \pi_2 = 0.07$; $\phi = 0.05$; $\mu = 0.0001$; $\beta = \gamma = 600$; and $k = 0.01$. In the left column, $\alpha = 0.0001$ and r increases from top to bottom as 0.002, 0.01, 0.05. In the right column, $r = 0.05$ and α increases from top to bottom as 0.0001, 0.001, 0.01.

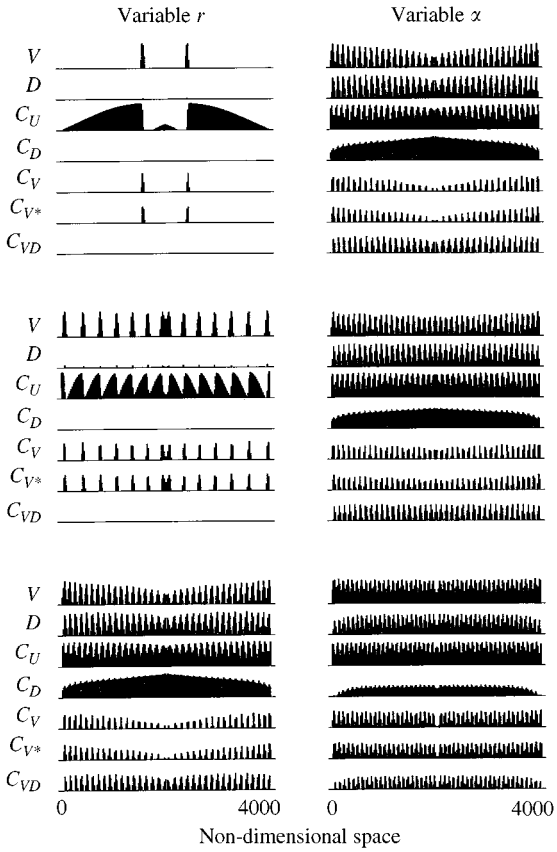

FIG. 4. Spatial pattern of the system in eqns (2) at the end of 5000 time units. Arrangement and parameters are the same as in Fig. 3. In addition, the spatial grid has 200 locations, and the distance between locations is $\Delta x = 20$, giving a total non-dimensional length of 4000.

host cells, reducing cellular death by viral virulence to low, oscillating levels.

The parameter α describes the rate of loss of DI particles from cells that lack V (C_D cells). The top-right panel of Fig. 3 has the same parameters as the lower-left panel. As α increases down the right column, DI particles are lost more quickly from C_D cells, causing a slight increase in the frequency and amplitude of cellular deaths by viral epidemics.

Figure 4 shows spatial dynamics for the same parameter combinations as Fig. 3. The qualitative effects are the same as in the spatially homogeneous case. Oscillations occur as moving bands of viremia. The distance between bands would, of course, be controlled by diffusion rate (not shown).

Other parameters influence dynamics as expected. For example, π_1 is the rate of transition between C_V and C_{V*} cells. The C_V cells are susceptible to infection by DI particles, whereas infection by a DI particle of C_{V*} is too late in the viral replication cycle to influence the production of V at burst. An increase in π_1 moves cells quickly out of the susceptible phase and reduces the abundance and potential controlling effects of DI particles. Infected organs with small spatial domains or high viral diffusion rates are more prone to viral extinctions because viral waves may travel out of the organ before the internal tissues can recover sufficiently to support a new wave.

Discussion

Many papers report the differing conditions that do or do not support widespread infection by DI particles. The reviews listed in the introduction summarize much of this literature. Here I mention one example to illustrate the state of the field. I then suggest that a comparative, testable theory can be developed from the models presented here. A comparative theory emphasizes how changes in key parameters predict changes in the dynamical outcomes of DI and wild-type viruses.

Holland *et al.* (1980, p. 167) reviewed the characteristics of persistently infected cell lines with and without DI particles. Carriers with DI particles included BHK cell lines with vesicular stomatitis virus (VSV) and BHK cells with rabies. Those without DI particles included L-cells with VSV and the HeLa–VSV–Car49 cell line.

Two demographic characteristics differed between cultured lines in which DI particles did and did not influence persistence. First, cells in which DI caused persistence had nearly 100% of cells with viral antigen, whereas those lines that did not require DI for persistence had a range of cells with viral antigen from 0 to 30%. Apparently, DI virus infects nearly all cells in the first case, greatly inhibiting the growth of the wild-type virus, whereas viral infection varies when DI virus is not involved. Second, persistent infections lasted many years when DI particles were involved. By contrast, without DI particles severe epidemics sometimes occurred, followed by loss of the virus and curing of the cell line.

My models have parameter combinations that match the observed differences. For example, DI particles are rare and clearance follows epidemic infections in the middle panel, left column of Fig. 3. The panel below has a higher rate of replacement for killed cells (higher r), a higher frequency of infection by DI particles (C_D), and more frequent but less severe epidemic outbreaks of cellular death. With higher values of r, virus persists indefinitely. Higher values of r moderate oscillations by replacing killed host cells quickly enough to keep host cell abundance above the level required to maintain virus. The virus, in turn, controls the increase in host cell abundance. Virus and host lock into persistent oscillations rather than bouts of epidemic catastrophe.

This fit of theory to observation shows that simple dynamical considerations could plausibly explain the data. But this fit by itself is not very convincing. The true value of the theory derives from its testable predictions. For example, relatively larger organs or organs with relatively lower rates of viral diffusion are more likely to support persistent infections. Small organs or high diffusion rates cause spatial waves of viremia to travel out the organ boundaries before new waves can develop in the interior.

The model also predicts that the rate of cellular replacement, r, strongly influences the role of DI particles. This could be tested experimentally by varying the conditions of the growth medium to modulate the rate of cellular division. If one could, for a particular cell line and virus, change the conditions that cause or prevent DI dominance, then one would have made a convincing case for the importance of cellular growth rate in explaining the wide diversity of outcomes observed.

I thank R. M. Bush for comments on the manuscript. National Science Foundation grant DEB-9627259 supports my research.

REFERENCES

ALLEN, L. J. S. (1983). Persistence and extinction in Lotka–Volterra reaction–diffusion equations. *Math. Biosci.* **65,** 1–12.

AMES, W. F. (1992). *Numerical Methods for Partial Differential Equations*, 3rd Edn. New York: Academic Press.

BANGHAM, C. R. M. & KIRKWOOD, T. B. L. (1990). Defective interfering particles: effects in modulating virus growth and persistence. *Virology* **179,** 821–826.

BANGHAM, C. R. M. & KIRKWOOD, T. B. L. (1993). Defective interfering particles and virus evolution. *Trends Microbiol.* **1,** 260–264.

BARRETT, A. D. T. & DIMMOCK, N. J. (1986). Defective interfering viruses and infections of animals. *Curr. Topics Microbiol. Immunol.* **128,** 55–84.

CAVE, D. R., HAGEN, F. S., PALMA, E. L. & HUANG, A. S. (1984). Detection of vesicular stomatitis virus RNA and its defective-interfering particles in individual mouse brains. *J. Virol.* **50,** 86–91.

CHEN, C.-J., BANERJEA, A. C., HARMISON, G. G., HAGLUND, K. & SCHUBERT, M. (1992). Multitarget-ribozyme directed to cleave at up to nine highly conserved HIV-1 env RNA regions inhibits HIV-1 replication-effectiveness against most presently sequenced HIV-1 isolates. *Nucl. Acid Res.* **17,** 4581–4589.

CHEN, M., HARTY, R. N., ZHAO, Y., HOLDEN, V. R. & O'CALLAGHAN, D. J. (1996). Expression of an equine herpesvirus 1 ICP22/ICP27 hybrid protein encoded by defective interfering particles associated with persistent infection. *J. Virol.* **70,** 313–320.

FISHER, R. A. (1937). The wave of advance of advantageous genes. *Ann. Eugenics* **7,** 355–369.
FRANK, S. A. (1994). Spatial polymorphism of bacteriocins and other allelopathic traits. *Evol. Ecol.* **8,** 369–386.
HASTINGS, A. (1978). Global stability of Lotka–Volterra systems with diffusion. *J. Math. Biol.* **6,** 163–168.
HOLLAND, J. J. (1990). Defective viral genomes. In: *Virology* (Fields, B. N., ed.), 2nd Edn, pp. 151–165. New York: Raven Press.
HOLLAND, J. J., KENNEDY, S. I. T., SEMLER, B. L., JONES, C. L., ROUX, L. & GRABAU, E. A. (1980). Defective interfering viruses and the host cell response. In: *Comprehensive Virology* (Fraenkel-Conrat, H. & Wagner, R. R., eds), Vol. 16, pp. 137–192. New York: Plenum.
HUANG, A. S. & BALTIMORE, D. (1977). Defective interfering animal viruses. In: *Comprehensive Virology* (Fraenkel-Conrat, H. & Wagner, R. R., eds), Vol. 10, pp. 73–116. New York: Plenum.
KIRKWOOD, T. B. L. & BANGHAM, C. R. M. 1994. Cycles, chaos, and evolution in virus cultures: a model of defective interfering particles. *Proc. Natl. Acad. Sci. U.S.A.* **91,** 8685–8689.
MURRAY, J. D. (1989). *Mathematical Biology*. New York: Springer-Verlag.
NELSON, G. W. & PERELSON, A. S. (1995). Modeling defective interfering virus therapy for AIDS: conditions for DIV survival. *Math. Biosci.* **125,** 127–153.
PERRAULT, J. (1981). Origin and replication of defective interfering particles. *Curr. Topics Microbiol. Immunol.* **93,** 151–207.
PRESS, W. H., TEUKOLSKY, S. A., VETTERLING, W. T. & FLANNERY, B. P. (1992). *Numerical Recipes in C*, 2nd Edn. Cambridge: Cambridge University Press.
ROUX, L., SIMON, A. E. & HOLLAND, J. J. (1991). Effects of defective interfering viruses on viral replication and pathogenesis *in vitro* and *in vivo*. *Adv. Virus Res.* **40,** 181–211.
SEGEL, L. A. (1972). Simplification and scaling. *SIAM Rev.* **14,** 547–571.
SEGEL, L. A. & Levin, S. A. (1976). Application of nonlinear stability theory to the study of the effects of diffusion on predator–prey interactions. In: *Topics in Statistical Mechanics and Biophysics: A Memorial to Julius L. Jackson, Proc. AIP Conf.*, (Piccirelli, R.A., ed.) Vol. 27, pp. 123–152. New York: American Institute of Physics.
SZATHMÁRY, E. (1993). Co-operation and defection: playing the field in virus dynamics. *J. theor. Biol.* **165,** 341–356.
TAKEUCHI, Y. (1986). Global stability in generalized Lotka–Volterra diffusion systems. *J. Math. Anal. Appl.* **116,** 209–221.
TWIZELL, E. H., WANG, Y. & PRICE, W. G. (1990). Chaos-free numerical solutions of reaction-diffusion equations. *Proc. Roy. Soc. Lond. A* **430,** 541–576.
VON MAGNUS, P. (1954). Incomplete forms of influenza virus. *Adv. Virus Res.* **2,** 59–79.

APPENDIX

Numerical Methods for PDEs

Numerical techniques for partial differential equations (PDEs) must be chosen according to the specific form of the equations (Ames, 1992). By contrast with ordinary differential equations or root-finding problems, which can often be solved by standard algorithms (Press *et al.*, 1992), a PDE system may require some modification of existing methods to fit the problem at hand. PDEs are also more difficult because of the computational burden of analysing dynamics in both space and time. Algorithms must therefore be computationally efficient as well as accurate.

To study eqns (2), I extended the method used by Twizell *et al.* (1990) for the Fisher (1937) equation, which is the classic growth and diffusion model for logistic dynamics of a single population. In particular, my extensions allow computationally efficient study of reaction–diffusion models for community dynamics. I developed this approach in my paper on bacteriocin dynamics (Frank, 1994). Here, I briefly outline my method and the specific equations used for analysis. See Press *et al.* (1992) and Ames (1992) for general background and definitions of PDE jargon, and Twizell *et al.* (1990) for more on the particular approach taken here.

The method uses the Crank–Nicolson scheme for spatial diffusion and a mixture of explicit and implicit difference terms for the reaction (viral infection, cellular growth, density dependent interactions among cells). In this approach, the new abundances in each time step, given by primed variables, are calculated from a mixture of the prior values (explicit terms) and the updated values (implicit terms). The mixed explicit–implicit finite difference equations for eqns (2) without the diffusion terms for V and D are

$$V' - V = (\beta\pi_2 C_{V^*} - V')\Delta t,$$

$$D' - D = (\gamma\phi C_{VD} - D')\Delta t,$$

$$C'_U - C_U = [rC_U(1 - C'_U - C_D - C_V - C_{V^*} - C_{VD}) - k(V + D)C'_U + \alpha C_D]\Delta t,$$

$$C'_D - C_D = (kDC_U - \alpha C'_D - kVC'_D)\Delta t,$$

$$C'_V - C_V = (kVC_U - \pi_1 C'_V - kDC'_V - \mu C'_V)\Delta t,$$

$$C'_{V^*} - C_{V^*} = (\pi_1 C_V - \pi_2 C'_{V^*})\Delta t,$$

$$C'_{VD} - C_{VD} = (kVC_D + kDC_V - \phi C'_{VD} + \mu C_V)\Delta t.$$

These equations are easily solved for the prime variables, providing simple calculations to update each variable in each iteration. For example, the solution for V' is

$$V' = \frac{V + \beta\pi_2 C_{V^*}\Delta t}{1 + \Delta t},$$

with similar solutions for the other variables.

Diffusion of viral particles requires an alternative approach for updating V and D in each iteration. Abundance at each spatial location must be analysed simultaneously. Here, I study only a single spatial dimension; the same principle applies to higher spatial dimensions.

The finite differences for V and D at location i are

$$\begin{aligned} V_i' - V_i &= (\beta\pi_2 C_{V^*} - V_i')\Delta t \\ &\quad + \lambda(1-\theta)(V_{i+1} - 2V_i + V_{i-1}) \\ &\quad + \lambda\theta(V_{i+1}' - 2V_i' + V_{i-1}'), \\ D_i' - D_i &= (\gamma\phi C_{VD} - D_i')\Delta t \\ &\quad + \lambda(1-\theta)(D_{i+1} - 2D_i + D_{i-1}) \\ &\quad + \lambda\theta(D_{i+1}' - 2D_i' + D_{i-1}'). \end{aligned}$$

The parameter θ determines the mixture between explicit (unprimed) and implicit (primed) values used to calculate the effects of spatial diffusion. I used the standard value of $\theta = \frac{1}{2}$, which is the Crank–Nicolson scheme. The spatial grid points i occur along a single dimension, where each non-dimensional spatial unit is divided into m intervals and thus $i = 0, \ldots, M$, where $M = mL$ for total non-dimensional length L. The boundaries are hostile, so that $V_i = D_i = 0$ for $i = 0, M$. The finite difference for the non-dimensional time step is Δt. Spatial grid length is subsumed in $\lambda = \Delta t/(\Delta x)^2$, where $\Delta x = 1/m$ is the non-dimensional grid length.

The mixture of implicit (primed) and explicit (unprimed) values in the reaction terms are chosen to increase stability (Twizell *et al.*, 1990) and to prevent the negative abundances that occur frequently in purely explicit schemes. In addition, this system can be put in a form that can be solved by efficient computational methods. All unprimed variables are known quantities from the current time step in the iterative procedure, so the only unknowns are the primed variables. From these equations the primed variables form a linear system of the form

$$\begin{aligned} &-\lambda\theta V_{i+1}' + (1 + \Delta t + 2\lambda\theta)V_i' - \lambda\theta V_{i-1}' \\ &\quad = \beta\pi_2 C_{V^*}\Delta t + \lambda(1-\theta)V_{i+1} \\ &\qquad + [1 - 2\lambda(1-\theta)]V_i + \lambda(1-\theta)V_{i-1}, \\ &-\lambda\theta D_{i+1}' + (1 + \Delta t + 2\lambda\theta)D_i' - \lambda\theta D_{i-1}' \\ &\quad = \gamma\phi C_{VD}\Delta t + \lambda(1-\theta)D_{i+1} \\ &\qquad + [1 - 2\lambda(1-\theta)]D_i + \lambda(1-\theta)D_{i-1}. \end{aligned}$$

This linear system is tridiagonal and can be solved with $O(N)$ calculations, allowing the study of large spatial grids (Press *et al.*, 1992).

I used open boundaries in all numerical studies, that is, I allowed diffusion off the ends of the spatial domain.

Dimensionality

I studied dynamics in a single spatial dimension in my numerical analyses. Extensive modeling of Lotka–Volterra and other ecological systems has been done for various spatial assumptions, including multiple spatial dimensions (e.g., Hastings, 1978; Allen, 1983; Takeuchi, 1986). Segel & Levin (1976) point out that, with a transition from one spatial dimension to two dimensions in their predator–prey models, two new phenomena may arise. First, smaller perturbations can disrupt locally stable equilibria in higher spatial dimensions. Second, novel spatial patterns can arise in equilibrium configurations in two dimensions relative to one dimension. Those novel equilibrium patterns have changing densities of variables over space. It would be interesting to extend the analyses of the DI system to compare the results with various classical ecological models.

Eigenvalues for System without DI Particles

The system in eqns (3) has the internal equilibrium given in eqns (4) when $\pi \neq 0$ and $k\beta > 1$. The Jacobian is

$$\mathbf{J} = \begin{pmatrix} -1 & 0 & \beta\pi \\ -kC_U & -rC_U & -rC_U \\ kC_U & kV & -\pi \end{pmatrix},$$

where the variables V and C_U are evaluated at the equilibrium given in eqns (4).

The characteristic equation is $\lambda^3 + a_1\lambda^2 + a_2\lambda + a_3 = 0$; noting that $k\beta C_U = 1$ at the internal equilibrium, the coefficients are

$$a_1 = 1 + rC_U + \pi,$$

$$a_2 = rC_U\,(1 + kV + \pi),$$

$$a_3 = kV(rC_U + \pi).$$

The Routh–Hurwitz conditions for stability require that all coefficients, a_i, be positive, and that $a_1a_2 > a_3$. All parameters and variables are positive, so the coefficients are all positive. The condition $a_1a_2 > a_3$ expands to

$$C_U[\pi^3 + (3 + r + rC_U)\pi^2 + (1 + 3rC_U + r^2C_U)\pi + rC_U + r^2C_U^2] > \pi^2.$$

Noting that $C_U = 1/k\beta$ at the internal equilibrium, either $3 + r > k\beta$ or $\pi > k\beta$ is sufficient to satisfy the inequality and guarantee local stability of the internal equilibrium. Increases in $k\beta$ and declines in r are destabilizing. Values of π greater than $k\beta$ and small values of π are stabilizing; values between these bounds can promote instability.